Polymer Chemistry

ROYAL SOCIETY OF CHEMISTRY

PAPER

View Article Online
View Journal | View Issue

Cite this: *Polym. Chem.*, 2023, **14**, 1536

Photochemically driven one-step triple dynamic network formation in printable tough hydrogel for self-healing tubular sensors†

Liwei Sun, Zhe Lu, Ping Zhang, Hongqiu Wei and You Yu *

Self-healing hydrogels have attracted widespread attention due to their excellent biocompatibility, mechanical properties, and reparability. However, it is still a challenge to construct in one step printable self-healing tough hydrogels (PSHTHs), which limits their advanced application. Here, we report a photochemically driven dynamic multinetwork formation (PDDMF) strategy for the one-step design of high-performance multinetwork PSHTHs. Orthogonal ruthenium photochemistry helps in the simultaneous formation of multiple covalent and dynamic networks in ~10 s. Triple dynamic networks of PSHTHs improve their mechanical performance and enable them to have excellent self-healing ability. These reversible hydrogen-bonded and ionically crosslinked networks could be healed in around 3 s after being destroyed at large shear strains (1000%). Also, PSHTHs exhibit 90% self-healing efficiency after multiple instances of mechanical damage and have mechanical performances similar to those of fresh samples. More importantly, this PDDMF strategy is controlled by simply adjusting the irradiation procedures and is compatible with standard extrusion printing technology to make complex 3D structures. As a proof-of-concept, highly sensitive tubular sensors are designed to detect environmental pressures anisotropically. It is anticipated that this PDDMF strategy and the as-prepared PSHTHs have potential applications in fabricating high-performance self-healing wearable devices, sensors, and bioelectronics.

Received 29th January 2023,
Accepted 6th March 2023

DOI: 10.1039/d3py00093a

rsc.li/polymers

Introduction

Human skin is a natural barrier that protects the body from injury, and an organ that senses subtle stimuli from external environments.[1–3] Achieving these functions depends highly on the skin's excellent mechanical properties, toughness, and signal transmission capability. Moreover, human skin can repair itself rapidly to recover its original functions when damaged. Such features have inspired the design of various biomimetic materials that mimic human skin for advanced applications.[4–10] Among these materials, hydrogels, which are porous, soft, and have adjustable mechanical properties,[11,12] are readily available to prepare skin-like materials for potentialuse in creating bionics,[13,14] tissue engineering,[15–17] wearable devices,[18–20] *etc*.

Regarding materials chemistry, the hierarchical epidermis, dermis, and hypodermis structure gives skin outstanding deformation, elasticity, and signal transmission properties over time. Reasonably, constructing multinetwork structures using hydrogels can mimic these properties to sense or resist external mechanical deformation.[21–23] Sequential polymerization generally prepares these high-performance hydrogels with double covalent networks and then post-treatment forms physically crosslinked networks in polymerized hydrogels. Contrasting and interpenetrating multinetworks in bulk hydrogels can significantly improve their mechanical properties (including fracture strength, toughness, anti-fatigue, *etc*.) through energy dissipation mechanisms.[24–27] Note that physically crosslinked networks are reversible and can be reconstructed after being destroyed by large strains. This recovery behavior gives hydrogels stable toughness under continuous large deformations. Moreover, this reversible destruction/construction process helps in designing self-healing hydrogels that maintain good mechanical performance and function under harsh conditions and even after damage.[28–33] Therefore, creating multiple dynamic networks in bulk hydrogel is possible to obtain high-performance skin-like soft materials. However, tedious multiple steps and long processing times are still required and limit the preparation of structured hydrogels using standard lithography and printing techniques. A straightforward and rapid strategy to design printable tough and self-healing hydrogels in one step is still an intriguing goal in this field.[34,35] As such, several issues should be con-

Northwest University, Xi'an, China. E-mail: yuyou@nwu.edu.cn

† Electronic supplementary information (ESI) available. See DOI: https://doi.org/10.1039/d3py00093a

sidered. First, most polymeric networks in hydrogels must be reversible, enabling them to have high self-healing efficiency under mild conditions. Second, multiple networks should be constructed simultaneously to permit the one-step formation of these hydrogels. Finally, the manner of the preparation process must be rapid and controlled to allow for the structural design of self-healing hydrogels using extrusion 3D-printing technology.

The present work reports a novel strategy of photochemically driven dynamic multinetwork formation (PDDMF) to design high-performance printable self-healing tough hydrogels (PSHTHs) in one step. The proposed ruthenium photochemistry is highly efficient and can simultaneously trigger different reactions in one pot for constructing multiple networks in seconds, including the radical polymerization of polyvinyl alcohol acetoacetate (PVAA), phenolic coupling of Gel-UPy and *in situ* release of Ca^{2+} from EDTA-Ca to form an ionic network with sodium alginate. The dynamic networks in hydrogels can not only improve their mechanical properties and energy dissipation but also enable excellent self-healing ability. Moreover, such a rapid preparation process is compatible with standard extrusion printing technology, making it possible to create complex 3D resistance sensors. To the best of our knowledge, this is the first time such a controlled and rapid strategy has been proposed for preparing PSHTHs with triple dynamic and self-healing networks.

Results and discussion

To date, many reversible bonds have been used to prepare self-healing hydrogels with multiple reversible networks.[33,36,37] Multiple hydrogen bonds and metal-coordinated bonds are easily synthesized and, therefore, widely employed to fabricate high-performance self-healing polymers.[32,38–40] However, the design bottleneck is how to design self-healing hydrogels with these different dynamic networks in a one-step controlled fashion. Orthogonal ruthenium photochemistry has been demonstrated as a powerful one-step strategy for constructing multiple networks in one hydrogel.[41,42] As a typical photochemistry, it enables precise spatial and temporal control of hydrogel formation compared with thermochemistry. Therefore, this combined rapid photochemistry reaction and controlled preparation process benefits complex structure design through standard lithography and 3D-printing techniques. Moreover, $[Ru(bpy)_3]^{2+}$ molecules are easily excited to the metal-to-ligand charge transfer (^{3}MLCT) excited state upon blue-light irradiation. The long-lived ^{3}MLCT state (~600 ns) allows these molecules to efficiently diffuse through solutions and react with other species.[43,44] This classic transition metal complex has high redox potentials and can cyclically catalyze various reactions when compared with common photoinitiators or chemicals. The whole process is achieved under mild conditions that do not require high temperatures, ultraviolet light or gamma rays, making it safe and biocompatible.[45] Based on these considerations, we believe that a new straightforward and time-saving method is available for addressing these issues by combining them with ruthenium photochemistry.

As shown in Fig. 1a, a PSHTH precursor is composed of *tert*-butyl acetoacetate-modified polyvinyl alcohol (PVAA), 2-ureido-4[1*H*]-pyrimidinone-modified gelatin (Gel-UPy), alginate (ALG), ethylenediaminetetraacetic calcium (EDTA-Ca), and tris(2,2′-bipyridyl)ruthenium(II) chloride/ammonium persulfate [Ru(II)/APS]. Under the irradiation of blue light (~452 nm), the Ru(II)/APS triggers three chemical reactions of phenol and acetoacetate coupling and photorelease of Ca^{2+} from EDTA-Ca (Fig. S1†).[46,47] The two coupling reactions make the hydrogel precursor gel in a short time. The released Ca^{2+} ions promote the formation of physically crosslinked networks *via* chelating with α-L-guluronic acid residues in ALG chains. As a result, three dynamical networks are constructed in PSHTHs in one step, which are based on quadruple H-bonds of UPy, multiple H-bonds of PVAA, and Ca^{2+}-crosslinked ALG, respectively. These multinetworks greatly improve the hydrogel mechanical performance compared to samples with single networks (Fig. 1b). The as-prepared PSHTH is strong, stretchable, and tough, but others are soft or brittle and cannot resist cutting treatment. The rapid and controllable preparation process is highly compatible with 3D extrusion printing to make hydrogel puzzles (Fig. 1c). Moreover, dynamic networks in PSHTHs enable them to have a good self-healing property under mild conditions. These cut pieces could merge after being rejoined for a predetermined time, and the healed hydrogel is as stretchable as the original. Thus, it is anticipated that this PDDMF strategy based on orthogonal ruthe-

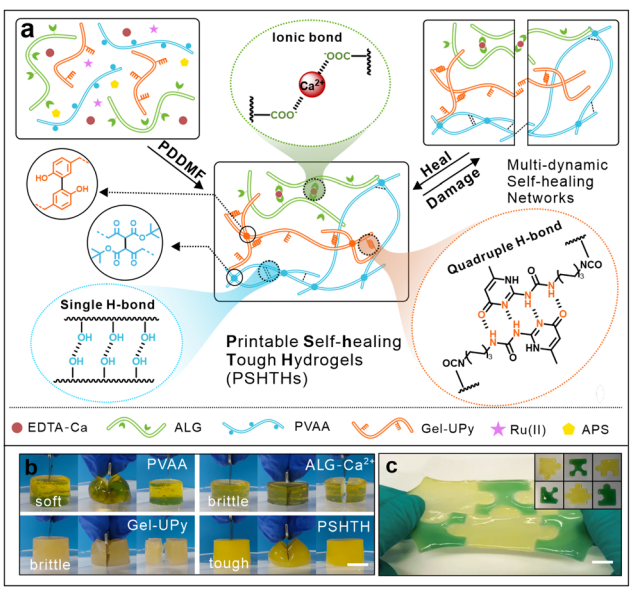

Fig. 1 Construction of PSHTHs *via* visible-light orthogonal photochemistry design. (a) The proposed schematic illustration for preparing multi-network self-healing hydrogels. Digital images of (b) PSHTH and hydrogels with a single component and (c) self-healing property of 3D printed PSHTH patterns (scale bar: 1 cm).

nium photochemistry is a straightforward method to design high-performance multinetwork self-healing hydrogels.

The chemical mechanism of the PDDMF strategy was systematically investigated by evaluating the effects of forming such high-performance hydrogels. The chemical mechanism of the PDDMF strategy was systematically investigated by evaluating the effects of components on PSHTHs. It can be seen from Fig. 2a that PSHTHs are tough and compressible, but the control samples are plastic or brittle. This result indicates that PVAA plays a critical role in the ability to form such high-performance hydrogels. First, rheology characterization was used to monitor the gelation process of PVAA (Fig. S2†). The acetoacetate coupling reaction significantly improved its mechanical property *via* ruthenium photochemistry. Therefore, the free *tert*-butyl acetoacetates (*t*-BAAs) were used as model molecules to further understand the coupling mechanism of PVAA. The UV-vis spectra in Fig. 2b and Fig. S3† indicate that the characteristic absorption of *t*-BAA keto–enol tautomerism gradually decreased with increasing irradiation time. The HPLC-MS characterization revealed that the content of this new substance also increased with prolonged time, and the corresponding molecular weight was ~337 g mol^{-1} (Fig. 2c and Fig. S4†).[48,49] The NMR spectra showed that another peak at ~4.3 ppm was generated, indicating a new kind of substance was synthesized after light irradiation. Moreover, a similar gelation reaction of *t*-BAA-modified PVA was initiated by APS under heat treatment (Fig. 2d and Fig. S5†). Reasonably, we believe that there is a sulfate radical-mediated reaction among *t*-BAA residues *via* the catalysis of ruthenium photochemistry (Fig. 2e).[50–52] Moreover, electron paramagnetic resonance (EPR) characterization was used to detect the generation of new radicals in precursor solutions upon light irradiation. The gradual increase in the intensity of the EPR signals between 3465 and 3555 G with increasing irradiation time indicated that *t*-BAAs were oxidized to carbon-centered radicals by the catalysis of ruthenium photochemistry (Fig. S6†).[53–56] Therefore, the possible reaction mechanism is as follows: APS is photodegraded into sulfate radicals by reacting with the excited Ru(II) under light irradiation. These intermediates can trigger the formation of *t*-BAA radicals in PVAA. As a result, PVAA hydrogels are obtained *via* the coupling reactions of *t*-BAA radicals. The gelation time (storage modulus (G') = loss modulus (G'')) reduces with increasing grafting ratios of *t*-BAA residues in PVAA (Fig. 2f). The shortest time of 5 s was observed in the sample with a *t*-BAA ratio of 7%. Moreover, this rapid coupling reaction greatly shortened the gelation time of PSHTHs from 45 s to 10 s and helped with its structural design in the extrusion 3D printing process (Fig. 2g). The PSHTH mesh maintained its predesigned high-resolution morphology, but a poor hydrogel was obtained with the *t*-BAA-free sample due to the slow gelation behavior after being extruded from the nozzle. Also, a comparison of the rheological characterizations revealed that introducing Gel-UPy and ALG shortened the gelation time of PSHTHs due to the phenol coupling of gelatin (Fig. S7–S9†) and Ca^{2+} crosslinking of ALG *via* such an orthogonal PDDMF strategy, respectively (Fig. 2h). Fig. 2i shows that Gel-UPy and ALG obviously improved the mechanical performance of hydrogels due to the formation of double networks when compared to that of the PVAA hydrogel with a single network. The combination of Gel-Upy and ALG gives PSHTHs the highest critical stress. Meanwhile, the strong multiple H-bonds of UPy residues endowed the Gel-UPy component with good stability at high temperatures and strains (Fig. S10†). The rigid ALG and Gel-UPy networks were interpenetrated with the soft PVAA network. The former two could dissipate energy quickly under large mechanical deformation, while the latter maintained its integrity.[57,58] As a result, the as-prepared PSHTHs were mechanically stable and showed similar behaviors during tests involving 200 cycles of continuous stretching (200% strain) and compressing (50% strain) (Fig. S11†).

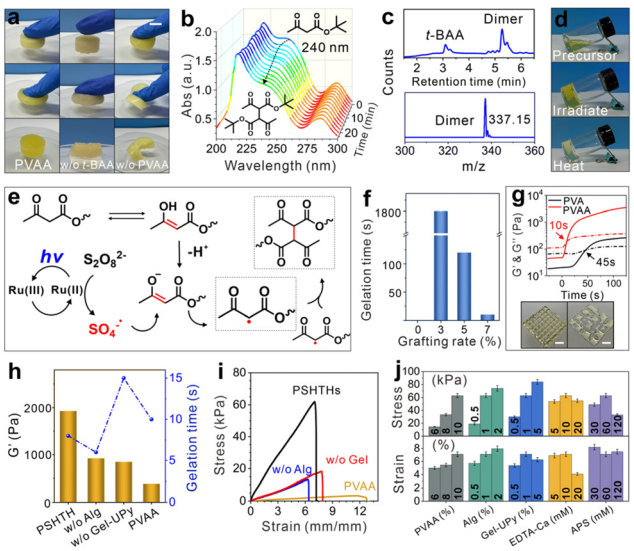

Fig. 2 (a) Digital images of PSHTHs (with PVAA), the control samples without t-BAA residues and PVAA, respectively (scale bar: 1 cm). (b) UV-vis characterization of the *t*-BAA solution with different irradiation times. (c) The HPLC-MS spectra of the resultant solutions (20 min of irradiation) in (b). (d) Digital images of PVAA gelation with different initiation methods of PVAA polymerization. (e) Photo-controlled reaction mechanism diagram of PVAA. (f) Gelation times of PVAA solution with different contents of *t*-BAA residues. (g) The rheology and 3D printing behaviors of PVA and PVAA solutions with external irradiation (scale bar: 5 mm). Effect of a single component on PSHTHs' (h) moduli and gelation times (G' = G'') and (i) mechanical properties. (j) The effect of component concentrations on the critical strain and stress of PSHTHs.

Moreover, the mechanical characterization of PSHTHs was applied to optimize their preparation conditions (Fig. 2j and Fig. S12†). Thus, if not especially mentioned, all PSHTHs were prepared under the following conditions: [PVAA] = 10 wt%, [Gel-UPy] = 5 wt%, [ALG] = 1 wt%, [EDTA-Ca] = 10 mM, [APS] = 60 mM and [Ru(II)] = 26.7 μM.

We found that there was a gel–sol transition at a shear strain of 950%, as shown in Fig. 3a, which indicated that multinetworks were destroyed under large deformation. However, G' and G'' of this hydrogel sample changed repeatedly as the shear strains were alternated between 1 and 1000%. This

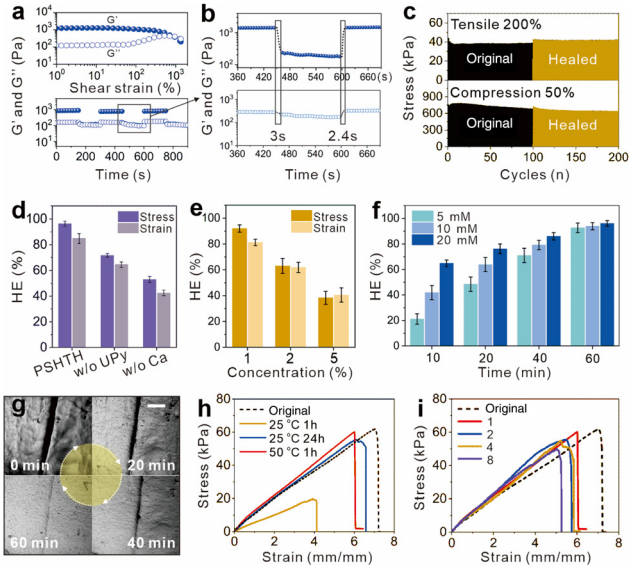

Fig. 3 (a) Shear–stress sweep tests of PSHTHs with strains ranging from 1 to 1000% and alternate strains of 1% and 1000%, respectively. (b) The response times to alternate strains of 1% and 1000%. (c) Continuous cyclic stretching and compressing tests of the original and healed PSHTHs. (d–f) Effect of UPy, EDTA-Ca and their specific concentrations on healing efficiencies. (g) Microscope images of PSHTHs at different healing times (scale bar: 50 μm). (h) Stress–strain curves of self-healed hydrogels with different healing temperatures and times. (i) Stress–strain curves of the original and healed PSHTHs after different healing times.

reversible destroy/recovery behavior was completed within a short time of 3 s (Fig. 3b). This self-healing behavior could be observed in each network (Fig. S13†). Furthermore, the healed samples had similar tensile and compression properties as the original samples after undergoing one hundred cycles of continuous tests (Fig. 3c and ESI Movie†). These results indicate that PSHTHs have good self-healing ability under mild conditions due to their multiple dynamic networks. The reversible H-bonds and metal coordination interaction enabled similar destruction and recovery behavior (Fig. S14†). All of the cut specimens were rejoined and healed and could be held using tweezers. Reasonably, these dynamic networks had noticeable effects on self-healing efficiencies of PSHTHs. The lack of quadruple H-bonds or metal-coordination interaction reduced the maximum stress and critical strains of the self-healed samples (Fig. 3d). But the higher content of UPy residues in Gel resulted in lower self-healing properties due to their rigid and poor mobility (Fig. 3e). The efficiency was reduced from >90% to ~40% when increasing the UPy content from 1 wt% to 5 wt%. As for Ca^{2+} ions, it was found that the self-healing efficiency was improved by increasing the content of EDTA-Ca in hydrogel precursors. Long healing times were helpful for the full diffusion of free Ca^{2+} and chelation with ALG in PSHTHs (Fig. 3f and Fig. S15†).[36] Therefore, we observed an almost five-fold increase in the efficiency when the healing time was prolonged to 60 min, even when the content of EDTA-Ca (5 mM) was low. The direct microscope observation also strongly confirmed this self-healing process; the size of the destroyed area decreased with increasing healing times. No obvious cutting trace was observed after 60 min of healing treatment (Fig. 3g). Moreover, increasing the self-healing temperature could accelerate the mobility of UPy residues, PVAA chains, and Ca^{2+} ions, leading to an increase in the self-healing efficiency of PSHTHs.[59] The comparison in Fig. 3h shows that the specific efficiency was only 36% when the control sample was healed at room temperature. Due to their excellent self-healing performance, PSHTHs exhibited similar self-healing efficiencies even after being subjected to eight rounds of cutting/healing treatment (Fig. 3i).

Besides the rapid gelation and self-healing property, Fig. 4a shows that the PDDMF strategy provides excellent controllability in PSHTH preparation. The storage moduli were effectively adjusted by treating the sample with interval irradiation in a spatial way. Thus, tubular PSHTHs were successfully made by combining this new PDDMF strategy and coaxial extrusion printing technique (Fig. 4b).[47] The precursor was extruded from nozzles (18G/12G) and exposed to visible light irradiation immediately, and the outer PSHTHs could seal the inner guest materials (*e.g.*, ethylene glycol). After dissolving, one-meter tubular PSHTH was obtained by continuously spinning 10 mL of the precursor from syringes (Fig. 4c). The structures of PSHTH tubes were easily regulated by simply controlling the applied air pressure. In addition, these tubes were self-healed as bulk samples and readily available for loading liquid sub-

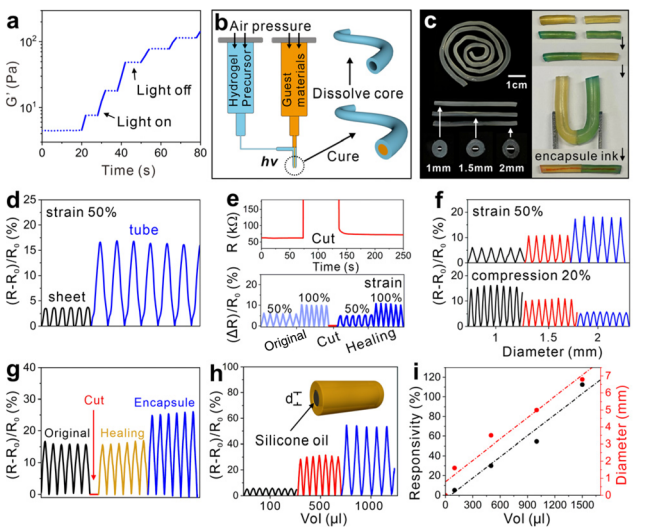

Fig. 4 (a) *In situ* rheology characterization (*G'*) of hydrogel precursors under intermittent light irradiation. (b) Schematic illustration of fabricating hydrogel tubes using a coaxial extrusion printing technique. (c) The digital images of the as-prepared tubular PSHTHs. (d) Resistance changes of PSHTH sheets and tubes under different strains. (e) Resistance changes of the original and healed hydrogel tubes under different strains. (f) Resistance changes of hydrogel tubes under 50% strain and 20% compression with different diameters. Resistance changes of hydrogel tubes under different (g) states and (h) volumes (d = 1 mm). (i) Relationship between responsivity, volume, and diameter (d = 1 mm).

stances (Fig. 4c and Fig. S16†). Specifically, the 3D structural design enhanced the resistance sensitivity, *i.e.*, $(R - R_0)/R_0$, of hydrogel tubes compared with the sheet sample due to greater deformation under the same tensile strain (Fig. 4d). Their sensitivity and conductivity performances were immediately restored when the tube was cut and healed (Fig. 4e). Also, it was found that these tubular PSHTHs had obvious anisotropic properties of resistance sensitivity in different deformation directions. The stretching sensitivity increased, but the compressing sensitivity decreased with increasing tube diameters (Fig. 4f). Furthermore, the sensitivity was improved by encapsulating hydrophobic silicone oil to regulate the PSHTH diameters (Fig. 4g). The specific values increased linearly with increasing oil volumes (Fig. 4h and 4i).

Conclusion

In summary, we report a straightforward and rapid PDDMF strategy to prepare PSHTHs in one step by combining orthogonal ruthenium photochemistry with rational structure design. These dynamic hydrogel networks significantly improve their mechanical performance and give them excellent self-healing properties. This PDDMF strategy is compatible with standard printing techniques and is applied to produce PSHTH sensors, which can differentiate deformation in different directions. Compared with other approaches, this PDDMF strategy has the following advantages. First, reversible H-bonds and Ca^{2+}–ALG interaction are successfully adopted to construct dynamic networks in hydrogels. Thus, typically reversible host–guest, electrostatic, hydrogen-bonding, and metal-coordinated interactions are also applicable for the preparation of versatile self-healing tough hydrogels with multinetworks *via* a similar strategy. Second, this rapid and controllable strategy is compatible with extrusion printing to make high-performance PSHTH tubes. Therefore, it could also be combined with typical photolithography, screen printing, and injection printing approaches for designing complex PSHTH patterns and structures. Third, the as-prepared PSHTHs are self-healing and sensitive to external change, which suggest applications for fabricating advanced self-healing devices and electronics. On the basis of these discussions, it is expected that this time-saving and facile strategy and the as-prepared PSHTHs will provide promising applications in the fields of biology, engineering, and materials chemistry.

Experimental

Materials

Tris(bipyridine)ruthenium(II) chloride [Ru(II), ACROS], polyvinyl alcohol [PVA, M_w ~145 000 g mol^{-1}, Aladdin], *tert*-butyl acetoacetate (*t*-BAA, 99%), guanidine carbonate, ethyl acetoacetate, hexamethylene diisocyanate, sodium alginate (180947, G/M = 1.02, Sigma-Aldrich), gelatin (Type A, ~300 g bloom from porcine skin, Sigma-Aldrich), polyquaternium-10 (JR-400, 1.6–2.1 N%), and other chemicals (Sinopharm Chemical Reagent Co. Ltd) were bought and used without further purification. Acetoacetate-modified PVA (PVAA), 2-amino-4-hydroxy-6-methylpyrimidine (UPy), 2(6-isocyanatohexylaminocarbonylamino)-6-methyl-4[1*H*]-pyrimidinone(UPy-NCO), and Gel-UPy were synthesized according to the reported methods, respectively.[38,60]

Synthesis of *t*-BAA dimer

t-BAA (0.316 M), Ru(II) (0.316 mM), and APS (0.316 M) were dissolved in 5 mL of DMSO. After being exposed to blue light at predetermined times, the products were purified by multiple hexane extractions and then dried in a vacuum for 6 h.

Fabrication of PSHTHs

In a typical fabricating process, 1 g of PVAA was fully dissolved in 10 mL of a mixed solution of DI water *via* rapid stirring at 70 °C. Different amounts of ALG, EDTA-Ca, and Gel-UPy (dissolved in 0.5 mL of DMSO) were then added, followed by magnetic stirring for 30 min at 50 °C until a homogeneous solution was achieved. After being cooled to room temperature, the catalyst of Ru(II) and APS was then added according to a predetermined concentration. The hydrogel precursor was finally obtained after completely dissolving the catalyst *via* magnetic stirring for ~5 min at room temperature. It should be noted that the whole process for the preparation of the precursor must proceed in a sealed container to prevent water evaporation. After degassing the precursor in a centrifuge at a rotating speed of 8000 rpm, it was cast into a Teflon mold to form PSHTHs by exposure to visible light.

3D printing of PSHTHs and fabrication of tubular hydrogels

3D printing of PSHTHs was basically conducted on a custom-designed 3D printer with a nozzle of 390 μm (22 G), a printing speed of 10 mm min^{-1}, and an applied pressure of around 0.2 MPa. All 3D structures are designed using Sketchup software. During the 3D-printing process, the prefabricated precursor was first mixed with a small amount (2 wt%) of hydroxyethylcellulose (Q10) to acquire suitable printing viscosity. The precursor was then put into a 10 mL syringe with a nozzle of the desired diameter after being degassed in the centrifuge at 8000 rpm. Next, the syringe was connected to the pressure supply and mounted on the head of the robot. PSHTH-based structures could be obtained by accurate control of the applied pressure, moving direction, and velocity of the robot with visible light irradiation. When fabricating the hydrogel tube, a coaxial nozzle (16G/12G) was used, and a highly viscoelastic aqueous ink of Q10 (10 wt%) was used as the sacrificial flow in the inner channel.

UV-vis spectroscopy testing

Ultraviolet spectra (PRESSE, TU-1810) were recorded to monitor the real-time polymerization of *t*-BAA under visible light (452 nm). The scan was performed every 90 s.

HPLC-MS testing

HPLC-MS analysis of the *t*-BAA dimer was performed using an Agilent Triple quadrupole mass spectrometer 6460 equipped with a C18 gravity column. The solvent is methanol.

Rheology testing

The gelation process of the hydrogel precursor under blue light was evaluated using a rotational rheometer (Anton Paar MCR302) assembled with optical modules and a 20 mm diameter steel parallel-plate geometry. The testing was conducted at room temperature with a strain of 1% at 10 Hz. Rheological characterization was performed after 1 min of equilibration.

Mechanical property testing

The mechanical tests of PSHTHs (10 mm × 50 mm × 1 mm) were performed on a tensile clamp (MTS, Insight 50) at a speed of 20 mm min^{-1} at room temperature.

Conductivity measurement

The sensitivity of PSHTHs was measured by a two-probe testing assembly with a digital multimeter (Keithley, 6517B). Three samples were tested for each composition. The sensitivity of the healed sample was measured after the hydrogel tubes were cut and spliced together and heated at 50 °C for 1 h. A hydrogel tube was filled with liquid and sealed with the precursor after illuminating.

Author contributions

The manuscript was written through contributions of all authors. All authors have given approval to the final version of the manuscript. All authors contributed equally.

Conflicts of interest

There are no conflicts to declare.

Acknowledgements

The authors acknowledge the National Natural Science Foundation of China (22175141 and 12102342), the Natural Science Foundation of Shaanxi Province (2023-JC-JQ-14 and 2022JQ-146) and the Young Elite Scientists Sponsorship Program by Xi'an Association for Science and Technology (095920221324) for the financial support of this work.

References

1 J. Chen, Y. Zhu, X. Chang, D. Pan, G. Song, Z. Guo and N. Naik, *Adv. Funct. Mater.*, 2021, **31**, 2104686.
2 B. Ying, R. Z. Chen, R. Zuo, J. Li and X. Liu, *Adv. Funct. Mater.*, 2021, **31**, 2104665.
3 M. Zhu, J. Li, J. Yu, Z. Li and B. Ding, *Angew. Chem., Int. Ed.*, 2022, **61**, e202200226.
4 E. K. Boahen, B. Pan, H. Kweon, J. S. Kim, H. Choi, Z. Kong, D. J. Kim, J. Zhu, W. B. Ying, K. J. Lee and D. H. Kim, *Nat. Commun.*, 2022, **13**, 7699.
5 S. Chen, L. Sun, X. Zhou, Y. Guo, J. Song, S. Qian, Z. Liu, Q. Guan, E. Meade Jeffries, W. Liu, Y. Wang, C. He and Z. You, *Nat. Commun.*, 2020, **11**, 1107.
6 T. Guan, X. Wang, Y.-L. Zhu, L. Qian, Z. Lu, Y. Men, J. Li, Y. Wang and J. Sun, *Macromolecules*, 2022, **55**, 5816–5825.
7 H. Yuk, T. Zhang, G. A. Parada, X. Liu and X. Zhao, *Nat. Commun.*, 2016, **7**, 12028.
8 J. Zhang, J. Li, W. Cheng, J.-H. Zhang, Z. Zhou, X. Sun, L. Li, J.-G. Liang, Y. Shi and L. Pan, *ACS Mater. Lett.*, 2022, **4**, 577–599.
9 W. Zhang, B. Wu, S. Sun and P. Wu, *Nat. Commun.*, 2021, **12**, 4082.
10 Q. Mu, K. Cui, Z. J. Wang, T. Matsuda, W. Cui, H. Kato, S. Namiki, T. Yamazaki, M. Frauenlob, T. Nonoyama, M. Tsuda, S. Tanaka, T. Nakajima and J. P. Gong, *Nat. Commun.*, 2022, **13**, 6213.
11 X. Zhao, X. Chen, H. Yuk, S. Lin, X. Liu and G. Parada, *Chem. Rev.*, 2021, **121**, 4309–4372.
12 Q. Mu, Q. Zhang, W. Yu, M. Su, Z. Cai, K. Cui, Y. Ye, X. Liu, L. Deng, B. Chen, N. Yang, L. Chen, L. Tao and Y. Wei, *ACS Appl. Mater. Interfaces*, 2020, **12**, 33152–33162.
13 S. Wei, H. Qiu, H. Shi, W. Lu, H. Liu, H. Yan, D. Zhang, J. Zhang, P. Theato, Y. Wei and T. Chen, *ACS Nano*, 2021, **15**, 10415–10427.
14 H. Yan, Y. Wang, W. Shen, F. Li, G. Gao, T. Zheng, Z. Xu, S. Qian, C. Y. Chen, C. Zhang, G. Yang and T. Chen, *Adv. Funct. Mater.*, 2022, **32**, 2203241.
15 F. Afghah, N. B. Iyison, A. Nadernezhad, A. Midi, O. Sen, B. Saner Okan, M. Culha and B. Koc, *Adv. Healthcare Mater.*, 2022, **11**, e2102068.
16 S. Tavakoli and A. S. Klar, *Biomolecules*, 2020, **10**, 1169.
17 H. Sun, M. Zhang, M. Liu, Y. Yu, X. Xu and J. Li, *Biomacromolecules*, 2020, **21**, 4699–4708.
18 C. Lim, Y. J. Hong, J. Jung, Y. Shin, S. H. Sunwoo, S. Baik, O. K. Park, S. H. Choi, T. Hyeon, J. H. Kim, S. Lee and D. H. Kim, *Sci. Adv.*, 2021, **7**, eabd3716.
19 M. S. Kim, Y. Lee, J. Ahn, S. Kim, K. Kang, H. Lim, B. S. Bae and I. Park, *Adv. Funct. Mater.*, 2022, **33**, 2208792.
20 S. Li, G. Liu, H. Wen, G. Liu, H. Wang, M. Ye, Y. Yang, W. Guo and Y. Liu, *Adv. Funct. Mater.*, 2022, **32**, 2111747.
21 J. P. Gong, Y. Katsuyama, T. Kurokawa and Y. Osada, *Adv. Mater.*, 2003, **15**, 1155–1158.
22 L. Xu, C. Wang, Y. Cui, A. Li, Y. Qiao and D. Qiu, *Sci. Adv.*, 2019, **5**, eaau3442.
23 F. Wu, Y. Pang and J. Liu, *Nat. Commun.*, 2020, **11**, 4502.
24 Y. Luo, M. Yu, Y. Zhang, Y. Wang, L. Long, H. Tan, N. Li, L. Xu and J. Xu, *Nano Energy*, 2022, **104**, 107955.
25 Y. R. Chen, X. Yan, F. Z. Yuan, L. Lin, S. J. Wang, J. Ye, J. Y. Zhang, M. Yang, D. C. Wu, X. Wang and J. K. Yu, *Adv. Sci.*, 2022, **9**, e2105571.

26 S. Choi, J. R. Moon, N. Park, J. Im, Y. E. Kim, J. H. Kim and J. Kim, *Adv. Mater.*, 2022, **35**, e2206207.
27 B. Ying, Q. Wu, J. Li and X. Liu, *Mater. Horiz.*, 2020, **7**, 477–488.
28 Z. Wang, H. Cui, M. Liu, S. L. Grage, M. Hoffmann, E. Sedghamiz, W. Wenzel and P. A. Levkin, *Adv. Mater.*, 2022, **34**, e2107791.
29 Z. Liu, H. K. Bisoyi, Y. Huang, M. Wang, H. Yang and Q. Li, *Angew. Chem., Int. Ed.*, 2022, **61**, e202115755.
30 X. Ding, G. Li, P. Zhang, E. Jin, C. Xiao and X. Chen, *Adv. Funct. Mater.*, 2021, **31**, 2011230.
31 B. Xue, H. Sheng, Y. Li, L. Li, W. Di, Z. Xu, L. Ma, X. Wang, H. Jiang, M. Qin, Z. Yan, Q. Jiang, J. M. Liu, W. Wang and Y. Cao, *Natl. Sci. Rev.*, 2022, **9**, nwab147.
32 M. Li, W. Li, W. Cai, X. Zhang, Z. Wang, J. Street, W.-J. Ong, Z. Xia and Q. Xu, *Mater. Horiz.*, 2019, **6**, 703–710.
33 Y. Li, L. Yang, Y. Zeng, Y. Wu, Y. Wei and L. Tao, *Chem. Mater.*, 2019, **31**, 5576–5583.
34 Z. Zhang, N. Corrigan and C. Boyer, *Angew. Chem., Int. Ed.*, 2022, **61**, e202114111.
35 M. Caprioli, I. Roppolo, A. Chiappone, L. Larush, C. F. Pirri and S. Magdassi, *Nat. Commun.*, 2021, **12**, 2462.
36 B. Li, Y. Zhang, Y. Han, B. Guo and Z. Luo, *Cellulose*, 2019, **26**, 6701–6711.
37 G. Su, S. Yin, Y. Guo, F. Zhao, Q. Guo, X. Zhang, T. Zhou and G. Yu, *Mater. Horiz.*, 2021, **8**, 1795–1804.
38 H. He, D. Li, Z. Lin, L. Peng, J. Yang, M. Wu, D. Cheng, H. Pan and C. Ruan, *Biofabrication*, 2020, **12**, 045003.
39 J. Xu, X. Wang, X. Zhang, Y. Zhang, Z. Yang, S. Li, L. Tao, Q. Wang and T. Wang, *Chem. Eng. J.*, 2022, **451**, 138673.
40 H. J. Won, B. Ryplida, S. G. Kim, G. Lee, J. H. Ryu and S. Y. Park, *ACS Nano*, 2020, **14**, 8409–8420.
41 C. Wang, P. Zhang, W. Xiao, J. Zhao, M. Shi, H. Wei, Z. Deng, B. Guo, Z. Zheng and Y. Yu, *Nat. Commun.*, 2020, **11**, 4694.
42 H. Wei, M. Lei, P. Zhang, J. Leng, Z. Zheng and Y. Yu, *Nat. Commun.*, 2021, **12**, 2082.
43 K. Kalyanasundaram, *Coord. Chem. Rev.*, 1982, **46**, 159–244.
44 D. M. Arias-Rotondo and J. K. McCusker, *Chem. Soc. Rev.*, 2016, **45**, 5803–5820.
45 D. M. Arias-Rotondo, *Nat. Chem.*, 2022, **14**, 716.
46 J. Liu, B. Zhang, P. Zhang, K. Zhao, Z. Lu, H. Wei, Z. Zheng, R. Yang and Y. Yu, *ACS Nano*, 2022, **16**, 17998–18008.
47 W. Xiao, P. Zhang, H. Wei and Y. Yu, *ACS Macro Lett.*, 2020, **9**, 1681–1686.
48 M. Galezowski and D. T. Gryko, *J. Org. Chem.*, 2006, **71**, 5942–5950.
49 A. Wu, Y. Zhao, N. Chen and X. Pan, *Synth. Commun.*, 2006, **27**, 331–336.
50 X. Wang, S. Chen, D. Wu, Q. Wu, Q. Wei, B. He, Q. Lu and Q. Wang, *Adv. Mater.*, 2018, **30**, e1705668.
51 J. P. Goddard, C. Ollivier and L. Fensterbank, *Acc. Chem. Res.*, 2016, **49**, 1924–1936.
52 T. L. D. Teixeira, M. Brigodiot and E. Marechal, *Macromolecules*, 1999, **32**, 70–72.
53 J. Y. Je, P. J. Park and S. K. Kim, *Food Chem. Toxicol.*, 2004, **42**, 381–387.
54 Q. Yang, T. Wang, F. Han, Z. Zheng, B. Xing and B. Li, *J. Alloys Compd.*, 2022, **897**, 163177.
55 Y. Zhou, X. Wang, C. Zhu, D. D. Dionysiou, G. Zhao, G. Fang and D. Zhou, *Water Res.*, 2018, **142**, 208–216.
56 X. Duan, C. Su, J. Miao, Y. Zhong, Z. Shao, S. Wang and H. Sun, *Appl. Catal., B*, 2018, **220**, 626–634.
57 R. E. Webber, C. Creton, H. R. Brown and J. P. Gong, *Macromolecules*, 2007, **40**, 2919–2927.
58 W. Sun, B. Xue, Q. Fan, R. Tao, C. Wang, X. Wang, Y. Li, M. Qin, W. Wang, B. Chen and Y. Cao, *Sci. Adv.*, 2020, **6**, eaaz9531.
59 F. M. Nie, C. H. An, D. F. Cao, J. Liu, Y. F. Zhou, Y. G. Lu, Z. Ma, L. Pan and Y. S. Li, *Adv. Funct. Mater.*, 2021, **32**, 2110616.
60 H. Liu, H. Yang, K. Zhu, F. Peng, L. Guo and H. Qi, *Mater. Horiz.*, 2022, **9**, 815–824.

